
Modeling correlations in spontaneous activity of visual cortex with centered Gaussian-binary deep Boltzmann machines

Nan Wang
Institut für Neuroinformatik
Ruhr-Universität Bochum
Bochum, 44780, Germany
nan.wang@ini.rub.de

Dirk Jancke
Institut für Neuroinformatik
Ruhr-Universität Bochum
Bochum, 44780, Germany
jancke@neurobiologie.rub.de

Laurenz Wiskott
Institut für Neuroinformatik
Ruhr-Universität Bochum
Bochum, 44780, Germany
laurenz.wiskott@rub.de

Abstract

Spontaneous cortical activity – the ongoing cortical activities in absence of sensory input – are considered to play a vital role in many aspects of both normal brain functions [1] and mental dysfunctions [2]. We present a centered Gaussian-binary deep Boltzmann machine (GDBM) for modeling the activity in visual cortex and relate the random sampling in DBMs to the spontaneous cortical activity. After training on natural image patches, the proposed model is able to learn the filters similar to the receptive fields of simple cells in V1. Furthermore, we show that the samples collected from random sampling in the centered GDBMs encompass similar activity patterns as found in the spontaneous cortical activity of the visual cortex. Specifically, filters having the same orientation preference tend to be active together during random sampling. Our work demonstrates the homeostasis learned by the centered GDBM and its potential for modeling visual cortical activity. Besides, the results support the hypothesis that the homeostatic mechanism exists in the cortex [3, 4].

1 Introduction

Spontaneous cortical activity has been studied in various contexts ranging from somato-sensory to visual and auditory perception [5]. These ongoing cortical activities in absence of sensory input are considered to play a vital role in many aspects of both normal brain functions [1], and mental dysfunctions [2]. Despite extensive studies of spontaneous activity, its role in brain still remains unclear. In [1], the spontaneous activity of visual cortex is reported to have a set of states, several of which resemble cortical representation of orientation, i.e. neurons in the visual cortex having similar orientation preference tend to be active together. One hypothesis is that biological agents learn to maintain homeostasis and avoid surprises in the sensory input by prediction [3]. From this perspective, the reported spontaneous cortical activity can be explained as the expected sensory inputs generated by the internal activity of the agents.

To understand the spontaneous activities of the visual cortex during hallucination, previous studies have considered Deep Boltzmann Machines (DBMs) as a potential model framework of the visual cortex and have related the inference in DBM to the mechanisms of cortical perception [6, 7]. The

authors have trained a DBM on binary images of simple shapes and have shown that trained DBMs can qualitatively reproduce several aspects of hallucination by maintaining its homeostasis. Following the same line of thinking, we have chosen a variant of DBM, a Gaussian-Binary DBM (GDBM), as a model for visual cortex. Adapting the centering trick [8] to GDBMs, we are able to make the model learn the homeostasis from natural image patches. The results suggest that centered GDBMs can be used to model the cortical activity in the primary visual cortex (V1) [1] and also support the hypothesis that the brain maintains a homeostasis [4].

In Section 2, the proposed centered GDBM is introduced. Then we describe the training procedure in Section 3.1, and show that the centered GDBM can not only learn Gabor-like filters, but also pick up more complex features in the higher layer. Finally, by considering the conditional probability of the hidden units during random sampling as the spontaneous activity, we show in Section 3.2 that these random samples present similar activity patterns as the spontaneous visual cortical activity reported in [1].

2 Algorithm

Like Deep Belief Networks (DBN) [9] and deep autoencoders [10], DBMs have been proposed for learning multi-layer representations that are increasingly complex. In particular, DBM incorporates both the top-down messages and the bottom-up passes during the inference for each layer, which gives DBM an advantage in propagating the input uncertainties. DBMs have been applied to many problems and show promising results[11, 12, 13].

To model the natural image patches that have continuous values, a variant of DBMs is required since the original DBM is designed for binary data. There are two common ways to extend DBMs to modeling continuous values. The most common way is to train a Gaussian-binary restricted Boltzmann machine (GRBM) as a preprocessing model and use the output of the trained model as the input data for training a DBM [14]. However, this practice loses the ability to train the model as a whole, i.e. the preprocessing part needs to be trained beforehand. A more natural extension is a Gaussian-binary deep Boltzmann machine (also known as Gaussian-Bernoulli DBM [15]), in which the binary units in the bottom layer are replaced by the real-value ones as in GRBMs. Moreover, GDBMs have been proved to be a universal approximator. The pitfall of GDBMs is the difficulty in training it [15].

The centering trick has been proposed in [8] for DBMs and has been shown to improve learning. Therefore, we adapted the centering trick to the GDBM and refer to the new model as centered GDBM. Compared with the training recipe in [15], a centered GDBM can easily be trained even without pre-training phase and is insensitive to the choice of hyper-parameters.

2.1 Centered GDBM

To avoid cluttering, we present a centered GDBM of two hidden layers as an example, although the model can be extended to an arbitrary number of layers. A two-layer centered GDBM, consisted of an input layer \mathbf{X} and two hidden layers, has an energy defined as:

$$\begin{aligned}
E(\mathbf{X}, \mathbf{Y}, \mathbf{Z}; \Theta, \mathcal{C}) : &= \sum_i^M \frac{(X_i - b_{X_i} - c_{X_i})^2}{2\sigma_i^2} - \sum_{i,j}^{L,M} \frac{(X_i - c_{X_i})w_{ij}(Y_j - c_{Y_j})}{\sigma_i^2} \\
&- \sum_j^M b_{Y_j}(Y_j - c_{Y_j}) - \sum_k^N b_{Z_k}(Z_k - c_{Z_k}) \\
&- \sum_{j,k}^{M,N} (Y_j - c_{Y_j})u_{jk}(Z_k - c_{Z_k}) \tag{1}
\end{aligned}$$

$$\begin{aligned}
&= \frac{(\mathbf{X} - \mathbf{c}_X - \mathbf{b}_X)^T \mathbf{\Lambda}^{-1} (\mathbf{X} - \mathbf{c}_X - \mathbf{b}_X)}{2} - (\mathbf{X} - \mathbf{c}_X)^T \mathbf{\Lambda}^{-1} \mathbf{W} (\mathbf{Y} - \mathbf{c}_Y) \\
&- (\mathbf{Y} - \mathbf{c}_Y)^T \mathbf{b}_Y - (\mathbf{Z} - \mathbf{c}_Z)^T \mathbf{b}_Z - (\mathbf{Y} - \mathbf{c}_Y)^T \mathbf{U} (\mathbf{Z} - \mathbf{c}_Z), \tag{2}
\end{aligned}$$

where \mathbf{Y} represents the first hidden layer, and \mathbf{Z} denotes the second hidden layer. L, M, N are the dimensionality of \mathbf{X}, \mathbf{Y} and \mathbf{Z} respectively. $\Theta := \{\mathbf{W}, \mathbf{U}, \mathbf{b}_X, \mathbf{b}_Y, \mathbf{b}_Z\}$ denotes the parameters trained for maximizing the loglikelihood. $\mathcal{C} := \{\mathbf{c}_X, \mathbf{c}_Y, \mathbf{c}_Z\}$ represents the centering parameters used to improve the learning. Λ is a diagonal matrix with the elements σ_i^2 . The probability of any given state $(\mathbf{x}, \mathbf{y}, \mathbf{z})$ in the DBM is

$$P(\mathbf{x}, \mathbf{y}, \mathbf{z}; \Theta, \mathcal{C}) : = \frac{1}{\mathcal{Z}(\Theta)} \exp(-E(\mathbf{x}, \mathbf{y}, \mathbf{z}; \Theta, \mathcal{C})). \quad (3)$$

Here $\mathcal{Z}(\Theta)$ is the partition function depended on the parameters of the model. Inference in centered GDBM is simple, because the states of the units in each layer are independent of the other ones in the same layer given the adjacent upper and lower layer.

$$P(X_i|\mathbf{y}) = \mathcal{N}(X_i; \mathbf{w}_{i*}(\mathbf{y} - \mathbf{c}_Y) + b_{X_i}, \sigma_i^2), \quad (4)$$

$$P(Y_j = 1|\mathbf{x}, \mathbf{z}) = f((\mathbf{x} - \mathbf{c}_X)^T \mathbf{w}_{*j} + \mathbf{u}_{j*}(\mathbf{z} - \mathbf{c}_Z) + b_{Y_j}), \quad (5)$$

$$P(Z_k = 1|\mathbf{y}) = f((\mathbf{y} - \mathbf{c}_Y)^T \mathbf{u}_{*k} + b_{Z_k}), \quad (6)$$

where $f(\cdot)$ is a sigmoid function and $\mathcal{N}(\cdot; \mu, \sigma^2)$ denotes a normal distribution with mean μ and variance σ^2 . \mathbf{w}_{i*} and \mathbf{w}_{*j} denote the i th row and the j th column of matrix \mathbf{W} . \mathbf{u}_{j*} and \mathbf{u}_{*k} are defined correspondingly.

For training a centered GDBM, the objective is to maximize the loglikelihood $\hat{\ell}$, of which the partial derivative for each parameter $\theta \in \Theta$ is

$$\frac{\partial \hat{\ell}}{\partial \theta} = \left\langle \frac{\partial(-E(\mathbf{x}, \mathbf{y}, \mathbf{z}))}{\partial \theta} \right\rangle_{data} - \left\langle \frac{\partial(-E(\mathbf{x}, \mathbf{y}, \mathbf{z}))}{\partial \theta} \right\rangle_{model}, \quad (7)$$

where $\langle \cdot \rangle_{data}$ and $\langle \cdot \rangle_{model}$ represent the expectation with respect to the data and the model distribution, respectively. By using the mean-field approximation, we can estimate the data-dependent expectation. And the model-dependent expectation is usually approximated by using persistent Markov Chains. See [14] for details.

As for the centering parameters, we adjust them along the training procedure with a moving average. In general, we follow the learning algorithm in [8] with several modifications as shown in Algorithm 1.

3 Experiments and results

3.1 Learning from natural image patches

We applied the centered GDBM to image patches of 32×32 pixels¹, taken randomly from the van Hateren natural image dataset [16]. The patches were firstly whitened by principal component analysis and reduced to the dimensionality of 256 in order to avoid aliasing [17].

Afterwards, we trained a centered GDBM with 256 visible units and two hidden layers. There were 900 units in the first hidden layer and 100 units in the second hidden layer². Despite the difficulties in training GDBMs, we found the centered GDBM can be trained much easier. Without any layer-wise pretraining, the centered GDBM did not suffer from the issue that the higher layer units are either always inactive or always active as reported in [15]. Since any centered GDBM can be reparameterized as a normal GDBM [19], this may imply that the centering trick in GDBM plays an important role in the optimization procedure.

¹We generated 60,000 image patches by randomly taken patches of 32×32 pixels from 2,000 natural images. A subset of size 50,000 was used for training. The rest was used for testing the reconstruction error and loglikelihood.

²The size of the hidden layers were chosen to get a good model of the spontaneous cortical activity as described in Section 3.2. The training procedure started with a learning rate of 0.03 and a momentum of 0.9, which is annealed to 0.001 and 0.0, respectively. But the standard deviation σ_i have a different learning rate, which is only one-tenth of the other's learning rate [18]. Neither weight decay nor sparse penalty is used during training. Mini-batch learning is used with a batch size of 100. The updating rate for centering parameters was 0.001. The training procedure was stopped when the reconstruction error stopped decreasing.

Algorithm 1 Training algorithm for centered GDBMs

```
1: Initialize  $\mathbf{W}, \mathbf{U}$       (i.e.  $w_{ij} \sim \mathcal{U}[-\sqrt{\frac{6}{L+M}}, \sqrt{\frac{6}{L+M}}], u_{jk} \sim \mathcal{U}[-\sqrt{\frac{6}{M+N}}, \sqrt{\frac{6}{M+N}}]$ )
2: Initialize  $\Lambda$       (i.e.  $\sigma_i^2 \sim \mathcal{N}(0.5, 0.01)$ )
3: Initialize  $\mathbf{b}_x, \mathbf{b}_y, \mathbf{b}_z$       (i.e.  $\mathbf{b}_x \leftarrow \langle \mathbf{x} \rangle_{data}, b_{y_j}, b_{z_k} \sim \mathcal{N}(-4.0, 0.01)$ )
4: Initialize  $\mathbf{c}_x, \mathbf{c}_y, \mathbf{c}_z$       (i.e.  $\mathbf{c}_x \leftarrow f^{-1}(\mathbf{b}_x), \mathbf{c}_y \leftarrow f^{-1}(\mathbf{b}_y), \mathbf{c}_z \leftarrow f^{-1}(\mathbf{b}_z)$ )
5: loop
6:    $\mathbf{y}_{model} \leftarrow \mathbf{c}_y$ 
7:   for all batches  $\mathbf{x}_{data}$  do
8:      $\mathbf{z}_{data} \leftarrow \mathbf{c}_z$ 
9:     loop
10:       $\mathbf{y}_{data} \leftarrow P(\mathbf{Y}|\mathbf{x}_{data}, \mathbf{z}_{data})$ 
11:       $\mathbf{z}_{data} \leftarrow P(\mathbf{Z}|\mathbf{y}_{data})$ 
12:      end loop until stop criteria is met
13:      loop
14:         $\mathbf{z}_{model} \sim P(\mathbf{Z}|\mathbf{y}_{model})$ 
15:         $\mathbf{x}_{model} \sim P(\mathbf{X}|\mathbf{y}_{model})$ 
16:         $\mathbf{y}_{model} \sim P(\mathbf{Y}|\mathbf{x}_{model}, \mathbf{z}_{model})$ 
17:        end loop until stop criteria is met
18:         $\mathbf{c}_x \leftarrow (1 - \nu) \cdot \mathbf{c}_x + \nu \cdot \langle \mathbf{x}_{data} \rangle$ 
19:         $\mathbf{c}_y \leftarrow (1 - \nu) \cdot \mathbf{c}_y + \nu \cdot \langle \mathbf{y}_{data} \rangle$ 
20:         $\mathbf{c}_z \leftarrow (1 - \nu) \cdot \mathbf{c}_z + \nu \cdot \langle \mathbf{z}_{data} \rangle$ 
21:         $\mathbf{W} \leftarrow \mathbf{W} + \eta(\langle (\mathbf{x}_{data} - \mathbf{c}_x)\Lambda^{-1}(\mathbf{y}_{data} - \mathbf{c}_y)^T \rangle - \langle (\mathbf{x}_{model} - \mathbf{c}_x)\Lambda^{-1}(\mathbf{y}_{model} - \mathbf{c}_y)^T \rangle)$ 
22:         $\mathbf{U} \leftarrow \mathbf{U} + \eta(\langle (\mathbf{y}_{data} - \mathbf{c}_y)(\mathbf{z}_{data} - \mathbf{c}_z)^T \rangle - \langle (\mathbf{y}_{model} - \mathbf{c}_y)(\mathbf{z}_{model} - \mathbf{c}_z)^T \rangle)$ 
23:         $\mathbf{b}_x \leftarrow \mathbf{b}_x + \eta(\langle \mathbf{x}_{data} \rangle - \langle \mathbf{x}_{model} \rangle) + \nu\Lambda^{-1}\mathbf{W}(\mathbf{y}_{data} - \mathbf{c}_y)$ 
24:         $\mathbf{b}_y \leftarrow \mathbf{b}_y + \eta(\langle \mathbf{y}_{data} \rangle - \langle \mathbf{y}_{model} \rangle) + \nu\mathbf{W}^T\Lambda^{-1}(\mathbf{x}_{data} - \mathbf{c}_x) + \nu\mathbf{U}(\mathbf{z}_{data} - \mathbf{c}_z)$ 
25:         $\mathbf{b}_z \leftarrow \mathbf{b}_z + \eta(\langle \mathbf{z}_{data} \rangle - \langle \mathbf{z}_{model} \rangle) + \nu\mathbf{U}^T(\mathbf{y}_{data} - \mathbf{c}_y)$ 
26:         $\mathbf{y}_{model} \leftarrow P(\mathbf{Y}|\mathbf{x}_{model}, \mathbf{z}_{model})$ 
27:      end for
28: end loop
```

After training, the centered GDBM had oriented, Gabor-like filters in the first hidden layer (Figure 1a). Most of the units in the second hidden layer had either strong positive or negative connections to the filters in the first layer that have similar patterns. As shown in Figure 1b, the filters having strong connections to the same second-layer units either have the similar orientation or the same location. The results also suggest that the model learned to encode more complex features such as contours, angles, and junctions of edges. These results resemble the properties of the neurons in V1 and V2 of visual cortex and imply that centered GDBM has a potential to be a good model for the visual cortex. Despite the resemblance of these results to those from sparse DBNs [20], sparse DBNs show worse match to the biological findings as reported in [1]. A quantitative comparison between centered GDBMs and sparse DBNs is still open for future studies.

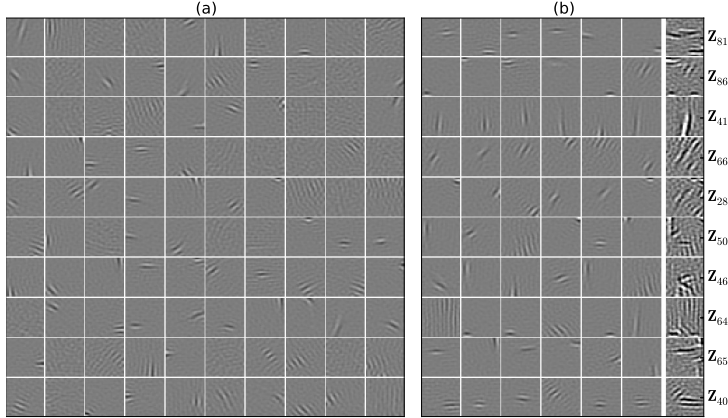


Figure 1: (a) 100 randomly selected first-layer filters learned from the natural image. (b) The leading six columns visualize the first-layer filters that have strongest connections to one selected second-layer unit. The filters are arranged from left to right in descending order by the absolute value of their weight to the selected unit. The last column depicts the weighted sum of the six strongest-connected filters, which can be considered as an approximation of the receptive fields of the selected second-layer units.

3.2 Comparing with biological experiments

After successful training of centered GDBM, we quantitatively analyzed the results of the trained model³ with the methods used in [1]. For conducting the measurements, we made two basic assumptions. Firstly, since only the first-layer filters of centered GDBM present strong orientation preferences, we assumed these filters correspond to the visual cortical neurons recorded in the literature. Secondly, the probability of the units to be active, i.e. $P(Y_j = 1|\mathbf{x}, \mathbf{z})$, was assumed to be the counterpart of the neuron’s activity.

3.2.1 Generating orientation maps

To compare with the original experiments, we firstly generated full-field gratings as input data and measured the response of the centered GDBM model. We collected the responses of the first-layer hidden units to eight orientations from 0° to 157.5° with a difference of 22.5° .

The amplitude of the gratings was chosen such that the average norm of the input stimuli is the same as that of the natural image patches before whitening. For each orientation, the grating stimuli of various frequencies and phases was fed to the model. We used the mean-field variational approximation to approximate the responses of the model to each stimulus. After collecting the responses, the average response over all the stimuli of each orientation were calculated and considered

³Considering the authors of the original paper [1] only presented the results from one hemisphere of a selected cat, here we only present the results of one centered GDBM that fits best to the reported results. However, all the centered GDBMs trained in our experience showed consistent results. In all the experiments, the strong correlation between the spontaneous frames and orientation maps can be observed as well as the emerging features presented in Figure 1.

to be the model’s response to the corresponding orientation. These activity patterns correspond to the *single-condition orientation maps* in [1]. Figure 2 (top) visualizes the most active filters in the single-condition orientation maps of four selected orientations.

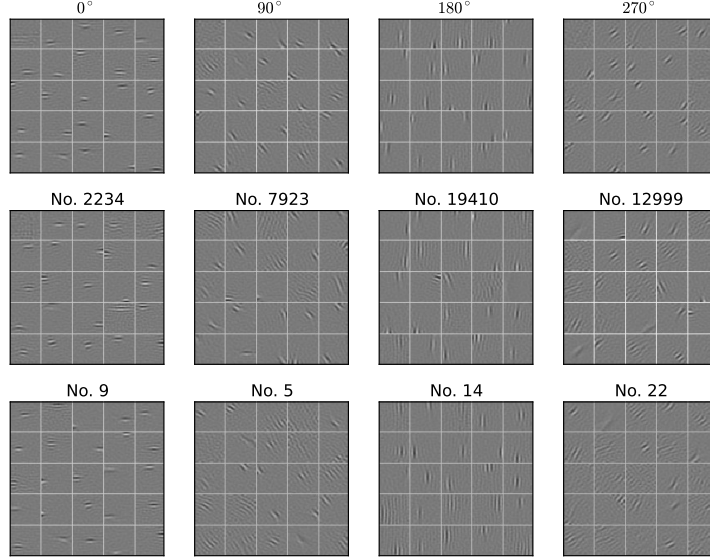


Figure 2: (top) The 25 most active filters in each of the four single-condition orientation maps. For each map the filters are arranged in a descending order of activity level. (middle) The same but using the filters in four spontaneous frames that are best correlated to the corresponding single-condition maps. (bottom) The same but using the filters of four best-correlated nodes in the self-organizing map.

3.2.2 Generating spontaneous frames

To simulate the spontaneously emerging cortical activity, we sampled the states of the trained model starting from a random initialization. In total, there were 200 Markov chains running Gibbs sampling for 2,000 iterations. For each Markov chain, the initial states of the hidden units in the first layer were set to be active with a probability that is equal to the average $P(\mathbf{Y}|\mathbf{x}, \mathbf{z})$ over the natural image patches. By recording the samples every 10 steps of Gibbs sampling, we collected 20,000 samples of $P(\mathbf{Y}|\mathbf{x}, \mathbf{z})$, which are referred as to *spontaneous frames*. Such a sampling procedure is referred to as a session. During the experiments we repeated the session for many times with every trained model.

3.2.3 Correlation between spontaneous frames and orientation maps

To establish the similarity between the single-condition orientation maps and the spontaneous frames, we calculated the spatial correlation coefficients between them. Figure 3(a) presents an example of the distribution of these correlation coefficients for four selected orientations⁴. For comparison, we generated random activity patterns of the first hidden layer with the same probability as the one used for initializing the Markov chains, and the same correlation coefficients were calculated with these random generated patterns. Although both distributions are center-peaked, those computed with spontaneous frames have much heavier tails, which indicates stronger correlation between the spontaneous frames and the single-condition orientation maps than expected by chances. The same observation were made in Figure 2 in [1].

⁴The following results were collected in a single session, but the results are consistent across simulation runs. In all sessions, the similar observation as shown in Figure 1–3 can be observed. The only difference is the shape of the curves in Figure 3b might vary in different sessions. However, the dominance of the cardinal orientation is always present.

We further calculated the orientation preference of these spontaneous frames. By this point, only the spontaneous frames that are significantly correlated were chosen. As in the biological experiment [1], we chose a significance level of $P < 0.01$, resulting in a threshold of $|0.182|$ and a selection of about 20% spontaneous frames. We then calculated the orientation preference of these frames by searching the orientation that is maximally correlated for each frame. Figure 3(b) plots the relative occurrences of the different orientation preferences together with the maximal correlation coefficients. The results match those from the cats' visual cortex in [1] fairly well.

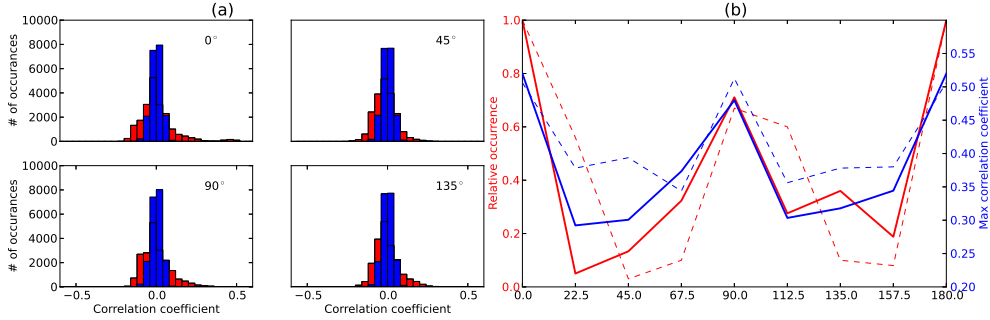


Figure 3: (a) Red, example distribution of the correlation coefficients between the spontaneous frames and the four selected single-condition orientation maps. Blue, the same, using random generated activity patterns with the same average probability. (b) The relationship between the relative occurrence of the different orientation preferences (red) and the maximal correlation coefficient (blue). The results from the centered GDBM are plotted by solid lines in comparison with the results in [1] plotted by dotted lines. The relative occurrence is calculated relative to the occurrence of the horizontal orientation. The figure is adapted to Figure 3b in [1].

Next we compared the most active filters in the spontaneous frames with those in the single-condition orientation map. Figure 2 (middle) visualizes these filters for four spontaneous frames that are best correlated with the selected single-condition orientation maps. These filters demonstrate similar features as those in the corresponding orientation maps shown in Figure 2 (top). This result further supports the similarity between the spontaneous frames and the orientation maps in centered GDBMs.

3.2.4 Learning SOM from the spontaneous frames

We followed the methods in [1] and applied Self-Organizing Map (SOM) algorithm [21] to the spontaneous frames in order to study the intrinsic structures of these spontaneous activities. We trained a SOM on the 20,000 spontaneous frames collected from a single session. The SOM projects the spontaneous frames onto 40 nodes that were arranged on a 1-D circle. See [1] for details of training. After training the SOM, we examined the correlation between the weight vectors of the 40 nodes and the single-condition orientation maps. Figure 2 (bottom) illustrates the most active filters in the weight vectors of four nodes that are best correlated with the selected single-condition orientation maps. The remarkable resemblance between these filters and those in the single-condition orientation maps suggests that the spontaneous frames encompass several states of the hidden variables in the first layer, which resemble the model's representation of orientation.

4 Discussion

To conclude, firstly we present a variant of DBMs, centered Gaussian-binary deep Boltzmann machines (GDBM) for modeling the activity in visual cortex. The proposed model applies the centering trick in [8] to the GDBMs and avoids the difficulties in training GDBMs. Moreover, the proposed centered GDBM does not require the layer-wise pretraining procedure⁵. An interesting question is

⁵Centering trick in normal DBMs is most successful in the DBMs of a few hundred hidden units[8]. However, in our experience, centered GDBM can always improve the learning of GDBMs.

how much benefit the centered GDBMs can provide in classification and generative performances. A further detailed comparison between centered and non-centered GDBM is currently being conducted.

Secondly, we consider centered GDBMs as a model of the visual cortex activity⁶. Compared to previous work [6], the proposed centered GDBM is able to model the natural image statistics from natural images patches. The hidden units in the centered GDBMs show V1 and V2 like receptive fields, which suggests a centered GDBM is a good model of the visual cortex.

Furthermore, we have found that the random samples of the first-layer hidden units encompass similar activity patterns as found in the spontaneous cortical activity of the visual cortex. Specifically, the hidden units having the same orientation preferences tend to be active together during random sampling procedure. On one hand, this result can be considered as a proof of the model's homeostasis learned from data. On the other hand, it also supports the hypothesis of homeostatic mechanisms in the cortex [4].

Acknowledgments

We would like to thank Jan Melchior for helpful comments. This work is funded by a grant from the German Research Foundation (Deutsche Forschungsgemeinschaft, DFG) to L. Wiskott (SFB 874, TP B3) and D. Jancke (SFB-874, TP A2).

⁶We've also conducted experiments with Gaussian-binary restricted Boltzmann machines, DBN with and without sparse penalty. None of these models can match the results in [1] as well as centered GDBMs. The correlation between the random samples and the orientation maps is significantly smaller than in centered GDBMs.

References

- [1] Tal Kenet, Dmitri Bibitchkov, Misha Tsodyks, Amiram Grinvald, and Amos Arieli. Spontaneously emerging cortical representations of visual attributes. *Nature*, 424:954–956, 2003.
- [2] W Burke. The neural basis of Charles Bonnet hallucinations: a hypothesis. *Journal of Neurology, Neurosurgery & Psychiatry*, 73(5):535–541, 2002.
- [3] Karl Friston. The free-energy principle: a unified brain theory? *Nature Reviews Neuroscience*, 11(2):127–138, 2010.
- [4] Gina G Turrigiano and Sacha B Nelson. Hebb and homeostasis in neuronal plasticity. *Current Opinion in Neurobiology*, 10(3):358 – 364, 2000.
- [5] Rémy Lestienne. Spike timing, synchronization and information processing on the sensory side of the central nervous system. *Progress in Neurobiology*, 65(6):545 – 591, 2001.
- [6] David Reichert, Peggy Series, and Amos Storkey. Hallucinations in Charles Bonnet syndrome induced by homeostasis: a deep Boltzmann machine model. In *the proceedings of the Conference on Neural Information Processing Systems (NIPS)*, pages 2020–2028, 2010.
- [7] David Reichert, Peggy Series, and Amos Storkey. Charles Bonnet syndrome: Evidence for a generative model in the cortex? *PLoS Comput Biol*, 9(7):e1003134, 07 2013.
- [8] Grégoire Montavon and Klaus-Robert Müller. Deep Boltzmann machines and the centering trick. In *Neural Networks: Tricks of the Trade*, volume 7700 of *Lecture Notes in Computer Science*, pages 621–637. Springer Berlin Heidelberg, 2012.
- [9] Geoffrey Hinton and Ruslan Salakhutdinov. Reducing the dimensionality of data with neural networks. *Science*, 313(5786):504–507, 7 2006.
- [10] Pascal Vincent, Hugo Larochelle, Yoshua Bengio, and Pierre-Antoine Manzagol. Extracting and composing robust features with denoising autoencoders. In *the proceedings of the International Conference on Machine Learning (ICML)*, pages 1096–1103. ACM, 2008.
- [11] Nitish Srivastava and Ruslan Salakhutdinov. Multimodal learning with deep Boltzmann machines. In *the proceedings of the Conference on Neural Information Processing Systems (NIPS)*, pages 2231–2239, 2012.
- [12] Nitish Srivastava, Ruslan Salakhutdinov, and Geoffrey Hinton. Modeling documents with deep Boltzmann machines. In *the proceedings of the International Conference on Uncertainty in Artificial Intelligence (UAI)*, 2013.
- [13] Ruslan Salakhutdinov, J Tenenbaum, and Antonio Torralba. Learning with hierarchical-deep models. *IEEE Transactions on Pattern Analysis and Machine Intelligence*, 35(8):1958–1971, 2013.
- [14] Ruslan Salakhutdinov and Geoffrey Hinton. Deep Boltzmann machines. In *the proceedings of the international conference on Artificial Intelligence and Statistics (AISTATS)*, volume 5, pages 448–455, 2009.
- [15] KyungHyun Cho, Tapani Raiko, and Alexander Ilin. Gaussian-Bernoulli deep Boltzmann machines. In *the proceedings of the International Joint Conference on Neural Networks (IJCNN)*, 2013.
- [16] A. van der Schaaf and J.H. van Hateren. Modelling the power spectra of natural images: Statistics and information. *Vision Research*, 36(17):2759 – 2770, 1996.
- [17] Aapo Hyvärinen, Juha Karhunen, and Erkki Oja. *Independent Component Analysis*. Adaptive and Learning Systems for Signal Processing, Communications and Control Series. Wiley, 2004.
- [18] Alex Krizhevsky. Learning multiple layers of features from tiny images. Master’s thesis, University of Toronto, Toronto, 4 2009.
- [19] Jan Melchior, Asja Fischer, Nan Wang, and Laurenz Wiskott. How to center binary restricted Boltzmann machines. *arXiv preprint arXiv:1311.1354*, 2013.
- [20] Honglak Lee, Chaitanya Ekanadham, and Andrew Y. Ng. Sparse deep belief net model for visual area v2. In *the proceedings of the Conference on Neural Information Processing Systems (NIPS)*. MIT Press, 2007.
- [21] Teuvo Kohonen. *Self-Organizing Maps*. Physics and astronomy online library. Springer Berlin Heidelberg, 2001.